

to appear in *Advances in Solid State Physics*, ed. by B. Kramer (Springer 2003)

Simulation of Transport and Gain in Quantum Cascade Lasers

A. Wacker¹, S.-C. Lee¹, and M.F. Pereira Jr.^{1,2}

¹ Institut für Theoretische Physik, Technische Universität Berlin, Hardenbergstr. 36, 10623 Berlin, Germany

² NMRC, Lee Maltings, Prospect Row, Cork, Ireland

Abstract. Quantum cascade lasers can be modeled within a hierarchy of different approaches: Standard rate equations for the electron densities in the levels, semiclassical Boltzmann equation for the microscopic distribution functions, and quantum kinetics including the coherent evolution between the states. Here we present a quantum transport approach based on nonequilibrium Green functions. This allows for quantitative simulations of the transport and optical gain of the device. The division of the current density in two terms shows that semiclassical transitions are likely to dominate the transport for the prototype device of Sirtori *et al.* but not for a recent THz-laser with only a few layers per period. The many particle effects are extremely dependent on the design of the heterostructure, and for the case considered here, inclusion of electron-electron interaction at the Hartree Fock level, provides a sizable change in absorption but imparts only a minor shift of the gain peak.

1 Introduction

Since the first realization of a quantum cascade laser (QCL) in 1994 [1] these semiconductor heterostructures have become important devices in the infrared regime operating up to room temperature [2]. Lasing in the THz-region was also achieved recently [3], opening a new window for applications. The standard devices contain an injector region guiding the electrons to the upper laser level in an active region where the optical transitions occur between a few discrete levels. A frequently studied prototype is the sample in [4]. Different designs are interminiband-QCLs [5,6], as well as QCLs without injector regions [7] or containing only four barriers per period like the staircase-laser [8] and a recent THz-QCL [9].

The modeling of quantum cascade lasers was first performed on the basis of rate equations [10] for the electron dynamics in the active region. It was assumed that the electrons reach the upper laser level with the rate J/e , where J is the current density and $e < 0$ is the electron charge. A necessary condition for inversion is that the scattering rate $1/\tau_{u \rightarrow l}$ from the upper to the lower laser level is smaller than the out scattering $1/\tau_l$ from the lower laser level. Optimizing these scattering rates by a sophisticated choice of well

and barrier widths in the active region, QCLs with high performance could be designed. While typically scattering with optical phonons is considered to be the main mechanism for the scattering rates [11,12], electron-electron scattering has also been treated [13,14]. The influence of a magnetic field has been studied by these rate equations in [15]. While these rate equations for the electron densities n_i [in units $1/\text{cm}^2$] for the levels i average over the momentum \mathbf{k} in the in-plane direction, the distribution functions $f_i(\mathbf{k})$ can be taken into account employing Monte-Carlo (MC) simulations [16–18].

If one includes the injector region in the simulation and imposes periodic boundary conditions (a good approximation as typical devices have approximately 30 periods each containing an active region and an injector region) a full simulation of QCL-devices can be performed. Such an approach was performed almost simultaneously on the basis of rate equations [19], MC-simulations [20] and a quantum transport model [21] obtaining good results for the current-voltage characteristic of a prototype device [4].

In this article we want to show, in how far quantum effects affect the transport and gain behavior and address the question if simple semiclassical models such as rate equations or MC-simulations are applicable. In particular we demonstrate (i) that the current can be calculated in a quantum transport model, (ii) how this relates to semiclassical approaches, and (iii) discuss the implications of many particle corrections on the gain spectra.

2 Current in Quantum Transport

In order to describe the quantum cascade laser we start by defining a set of single particle basis states $\Psi_\alpha(z)e^{i\mathbf{k}\cdot\mathbf{r}}/\sqrt{A}$. Here \mathbf{k}, \mathbf{r} are two dimensional vectors in the x, y plane perpendicular to the growth direction z and A is the normalization area. The functions $\Psi_\alpha(z)$ reflect the layer sequence of the QCL structure and may be chosen as energy-eigenstates or Wannier states (see the discussion in [22]). Then the Hamilton operator reads in second quantization:

$$\hat{H} = \underbrace{\sum_{\alpha, \beta, \mathbf{k}, s} H_{\alpha\beta}^o(\mathbf{k}) a_{\alpha, \mathbf{k}}^\dagger a_{\beta, \mathbf{k}}}_{\hat{H}^o} + \hat{H}_{\text{scatt}} \quad (1)$$

where all terms connecting different \mathbf{k} -indices (i.e. breaking the translational invariance of the structures) have been included in \hat{H}_{scatt} . The spin index s yields an additional factor 2 for the current and the gain as we assume that all states are spin degenerate and no spin transitions occur.

Much information is contained in the (reduced) density matrix

$$\rho_{\alpha\mathbf{k}, \beta\mathbf{k}'} = \langle \hat{a}_{\beta, \mathbf{k}'}^\dagger \hat{a}_{\alpha, \mathbf{k}} \rangle; \quad (2)$$

in particular the occupation probabilities are given by the diagonal elements $f_\alpha(\mathbf{k}) = \rho_{\alpha\mathbf{k}\alpha\mathbf{k}}$. The average current density (in the z -direction) is evaluated

by the temporal evolution of the position operator \hat{z}

$$J = \frac{e}{V} \left\langle \frac{d}{dt} \hat{z} \right\rangle = \underbrace{\frac{e}{V} \frac{i}{\hbar} \langle [\hat{H}^o, \hat{z}] \rangle}_{=J_0} + \underbrace{\frac{e}{V} \frac{i}{\hbar} \langle [\hat{H}_{\text{scatt}}, \hat{z}] \rangle}_{=J_{\text{scatt}}}, \quad (3)$$

where V denotes the normalization volume. Let us first consider the current J_0 . For an arbitrary choice of the basis we may write

$$J_0 = 2(\text{for Spin}) \frac{e}{V} \sum_{\alpha\beta\mathbf{k}} \frac{i}{\hbar} W_{\beta,\alpha}(\mathbf{k}) \rho_{\alpha\mathbf{k},\beta\mathbf{k}} \quad (4)$$

where

$$W_{\beta,\alpha}(\mathbf{k}) = \sum_{\gamma} H_{\beta\gamma}^o(\mathbf{k}) z_{\gamma\alpha} - z_{\beta\gamma} H_{\gamma\alpha}^o(\mathbf{k}) \quad (5)$$

is an anti-hermitian matrix. If the wave functions $\Psi_{\alpha}(z)$ are chosen real, which is typical for bound states, $W_{\beta,\alpha}(\mathbf{k})$ becomes real and J_0 is determined by the non-diagonal elements of $\rho_{\alpha\mathbf{k},\beta\mathbf{k}}$.

For a scattering part of the form

$$\hat{H}_{\text{scatt}} = \sum_{\alpha\gamma\mathbf{k},\mathbf{k}',s} \hat{O}_{\alpha\mathbf{k},\gamma\mathbf{k}'}(t) \hat{a}_{\alpha\mathbf{k}}^{\dagger}(t) \hat{a}_{\gamma\mathbf{k}'}(t), \quad (6)$$

which contains only pairs of electronic annihilation and creation operators, we obtain

$$J_{\text{scatt}} = \frac{2e}{V\hbar} \sum_{\alpha\mathbf{k}} \sum_{\gamma\beta\mathbf{k}'} i \left\langle \hat{a}_{\alpha\mathbf{k}}^{\dagger} \left[\hat{O}_{\alpha\mathbf{k},\beta\mathbf{k}'}(t) z_{\beta\gamma} - z_{\alpha\beta} \hat{O}_{\beta\mathbf{k},\gamma\mathbf{k}'} \right] \hat{a}_{\gamma\mathbf{k}'} \right\rangle. \quad (7)$$

In the case of phonon scattering $\hat{O}_{\alpha\mathbf{k},\gamma\mathbf{k}'}$ contains phonon annihilation and creation operators and thus phonon-assisted density matrices [23] determine J_{scatt} for this scattering process.

To evaluate the density matrices we perform the perturbation expansion within the formalism of nonequilibrium Green functions [24–26] similar to [27]. The key quantities are the lesser and retarded Green function

$$G_{\alpha_1,\alpha_2}^{<}(\mathbf{k}; t_1, t_2) = i \langle a_{\alpha_2\mathbf{k}}^{\dagger}(t_2) a_{\alpha_1\mathbf{k}}(t_1) \rangle \quad (8)$$

$$G_{\alpha_1,\alpha_2}^{\text{ret}}(\mathbf{k}; t_1, t_2) = -i\Theta(t_1 - t_2) \langle a_{\alpha_1\mathbf{k}}(t_1) a_{\alpha_2\mathbf{k}}^{\dagger}(t_2) + a_{\alpha_2\mathbf{k}}^{\dagger}(t_2) a_{\alpha_1\mathbf{k}}(t_1) \rangle \quad (9)$$

where the time dependence is taken in the Heisenberg picture. The lesser Green function refers to the electron density and it becomes the density matrix $\rho_{\alpha_1\mathbf{k},\alpha_2\mathbf{k}}(t) = G_{\alpha_1,\alpha_2}^{<}(\mathbf{k}; t, t)/i$ for equal times. In the stationary state considered here the Green functions only depend on the time difference $t = t_1 - t_2$ and we introduce the energy E as the Fourier conjugate of t :

$$G(t_2 + t, t_2) = \int \frac{dE}{2\pi} G(E) e^{-iEt/\hbar} \quad (10)$$

This provides us with the Dyson equation

$$(E - \mathbf{H}^o(\mathbf{k}) - \boldsymbol{\Sigma}^{\text{ret}}(\mathbf{k}, E)) \mathbf{G}^{\text{ret}}(\mathbf{k}, E) = \mathbf{1} \quad (11)$$

and the Keldysh relation

$$\mathbf{G}^<(\mathbf{k}, E) = \mathbf{G}^{\text{ret}}(\mathbf{k}, E) \boldsymbol{\Sigma}^<(\mathbf{k}, E) \mathbf{G}^{\text{adv}}(\mathbf{k}, E) \quad (12)$$

where capital bold symbols represent matrices in $\alpha\beta$. Together with the functionals $\boldsymbol{\Sigma}\{\mathbf{G}\}$ for the self-energies this provides a self consistent set of equations which can be solved numerically. Although the Green functions are diagonal in \mathbf{k} , the expression (7) for J_{scatt} can be evaluated by Eq. (21) as derived in the appendix.

Here we use self-energies in self-consistent Born approximation for impurity, interface roughness, and phonon scattering, applying the following approximations: (i) The \mathbf{k} -dependence of the scattering matrix elements is neglected. (ii) It is assumed that $\boldsymbol{\Sigma}$ is diagonal and depends only on the diagonal elements of \mathbf{G} in the basis of Wannier functions. The scattering matrix elements are evaluated for a typical momentum transfer assuming an interface roughness with average height of $0.28/\sqrt{2\pi} \text{ nm}^{-1}$ and a correlation length of 10 nm. The impurity scattering was estimated by an effective scattering rate $\gamma_{\text{imp}}/\hbar$. Electron-electron interaction is included within the mean field approximation. See [22] for further details.

3 The Current-Voltage Characteristic

We perform our calculation using a basis of Wannier functions. These functions are shown in Fig. 1 for zero bias and an operating field of 220 mV per period for the sample used in [4]. While the spatial structure of the Wannier functions does not change with bias, their energetic position is affected both by the external field and the mean field which is evaluated self consistently. From Fig. 1 we see, that the mean field almost vanishes at operating conditions as the electrons are mainly in the injector region where the doping is also located. The energy levels of the Wannier functions bunch at the operating field indicating the strong coupling between the functions enabling transport through the structure.

In Fig. 2 the current-voltage characteristic is shown for different doping densities N_D per period. The theoretical result exhibits a monotonic increase of the current density with doping, showing that the mean field has no dramatic influence on the transport behavior in these structures. We find good agreement with the experimental data except for $N_D = 3.5 \times 10^{11}/\text{cm}^2$ and $N_D = 5.3 \times 10^{11}/\text{cm}^2$ where the experiment exhibits a significantly higher bias drop. The difference is of the same order as the bias of a test structure

¹ In the calculations performed in [22] a factor 2π was lacking in the program, which can be compensated by the reduction in the roughness height.

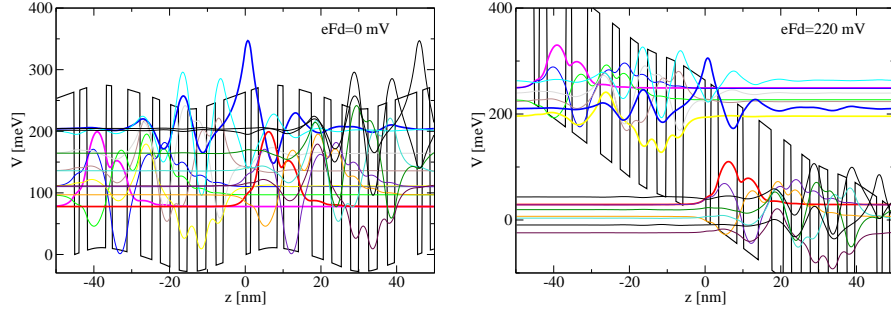


Fig. 1. Conduction band offset including mean field potential and Wannier functions for two different electric fields for the sample of [4]

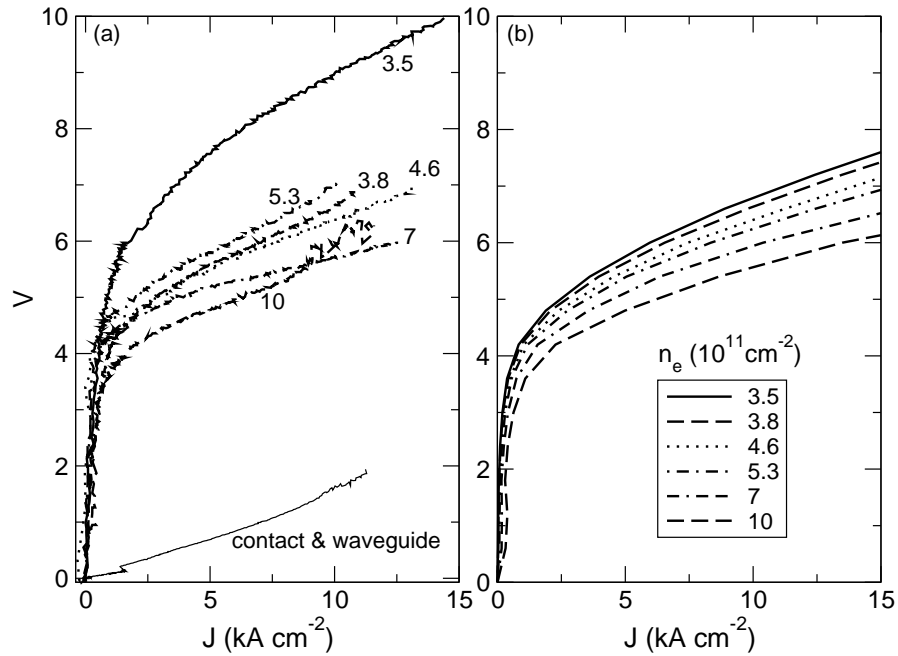


Fig. 2. Current-voltage characteristics for different doping densities for the structures of [28] at $T = 77$ K. **(a)** Experimental data from M. Giebler (PDI Berlin) where the thin line refers to a structure grown without the QCL structure, thus providing an estimate for contact effects. **(b)** Theoretical result for $\gamma_{\text{imp}} = 5$ meV using the bias $U = NFd$, where the QCL structure consists of $N = 30$ periods

containing only contact layers and the waveguides, albeit it is not clear why this additional bias drop is only present in some samples.

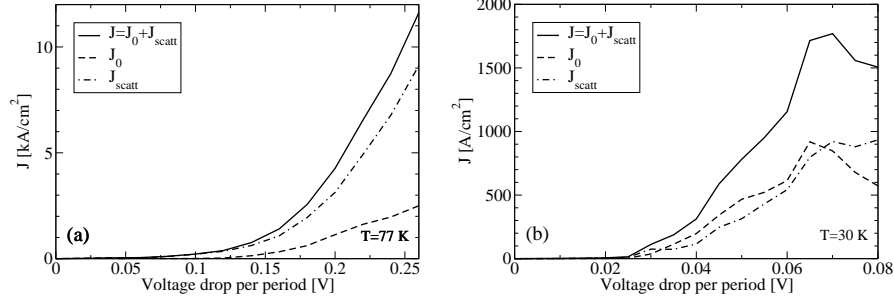


Fig. 3. Contributions to the current density for the samples of [4] (a) and [9] (b). $\gamma_{\text{imp}} = 0$ was used in the calculations

4 Comparing J_0 and J_{scatt}

In Fig. 3(a,b) we show the different contributions to the current evaluated for the structures of [4] and [9], respectively. Both current-field relations are in reasonable agreement with the respective experimental results. (The data of [9] only extends to $Fd \approx 70$ mV, therefore there is no verification of the current peak.) While J_{scatt} dominates the behavior in Fig. 3a, both the contributions of J_0 and J_{scatt} are important in Fig. 3b.

In the following we want to discuss the role of the two current contributions with respect to the use of semiclassical approaches: As the expressions for J_0 and J_{scatt} are invariant to unitary transformations of the basis states, they can be evaluated in arbitrary basis sets. A special basis set is given by the energy eigenstates $\varphi_\mu(z)$ obtained by diagonalizing \hat{H}^o (including the mean field), which will be used in the following argumentation.

The semiclassical theories used in [19,20] imply that the density matrix is diagonal in the energy eigenstates, i.e., $\rho_{\mu\mathbf{k}\mu'\mathbf{k}} = \delta_{\mu\mu'} f_\mu(\mathbf{k})$. In this basis the diagonal elements of $W_{\mu\mu'}$ in Eq. (5) vanish and thus J_0 becomes zero in the semiclassical approximation.

In the semiclassical approximation the Green functions in the basis of energy eigenstates are given by

$$G_{\mu,\nu}^{\text{ret/adv}}(\mathbf{k}, E) \approx \mp \pi i \delta_{\mu,\nu} \delta(E - E_\mu) \quad (13)$$

$$G_{\mu,\nu}^<(\mathbf{k}, E) \approx 2\pi i \delta_{\mu,\nu} \delta(E - E_\mu) f_\mu(\mathbf{k}) \quad (14)$$

Then we find from Eq. (21)

$$J_{\text{scatt}} \approx \frac{2e}{V\hbar} \sum_{\mu\mathbf{k}} \left\{ \frac{i}{2} \Sigma_{\mu\mu}^< z(\mathbf{k}, E_\mu) + i f_\mu(\mathbf{k}) \Sigma_{\mu\mu}^{\text{ret}} z(\mathbf{k}, E_\mu) - \sum_{\nu} z_{\mu\nu} \left[\frac{i}{2} \Sigma_{\nu\mu}^<(\mathbf{k}, E_\mu) + i f_\mu(\mathbf{k}) \Sigma_{\nu\mu}^{\text{ret}}(\mathbf{k}, E_\mu) \right] \right\} \quad (15)$$

In semiclassical approximation the self-energies are related to the scattering probabilities $R_{\mu'\mathbf{k}'\rightarrow\mu\mathbf{k}}$ as follows

$$\Sigma_{\mu\mu}^<(\mathbf{k}, E_\mu) = i\hbar \sum_{\mu'\mathbf{k}'} f_{\mu'}(\mathbf{k}') R_{\mu'\mathbf{k}'\rightarrow\mu\mathbf{k}}, \quad \Sigma_{\mu\mu}^{\text{ret}}(\mathbf{k}, E_\mu) = -\frac{i}{2}\hbar \sum_{\mu'\mathbf{k}'} R_{\mu\mathbf{k}\rightarrow\mu'\mathbf{k}'}$$

and the quantities $\Sigma^{<z}$ and $\Sigma^{\text{ret}z}$ contain an additional factor $z_{\mu'\mu'}$. This provides us with

$$J_{\text{scatt}} \approx \frac{2e}{V} \sum_{\mu\mathbf{k}\mu'\mathbf{k}'} R_{\mu\mathbf{k}\rightarrow\mu'\mathbf{k}'} (z_{\mu'\mu'} - z_{\mu\mu}) \quad (16)$$

which is the semiclassical expression for the current density². Therefore the entire current is contained in J_{scatt} in the semiclassical approximation.

For the special case of the structure considered in [4], the density matrix is approximately diagonal in the basis of energy eigenstates³ implying that $J_0 \rightarrow 0$ and J_{scatt} is well approximated by the semiclassical expression (16). This expectation is supported by Fig. 3a and the findings of [20]. In contrast, J_0 is an important contribution for the THz-laser of [9], which contains only 4 barriers per period, see Fig. 3b. Therefore it is questionable if semiclassical approaches work here.

5 Gain and Absorption Spectra

The general evaluation of gain spectra within the quantum transport model used here was described in detail in [29]. The key idea is to evaluate the complex susceptibility $\chi(\omega)$ which is related to the optical absorption coefficient at a frequency ω via [30]

$$\alpha(\omega) = \frac{\omega}{c} \frac{\Im\{\chi(\omega)\}}{n_B}, \quad (17)$$

where n_B is the background refractive index and c is the speed of light. Figure 4 shows the gain spectrum for the sample of [4]. At zero current we find strong absorption due to transitions in the active region, which vanishes already for small currents as the carriers are transferred to the injector region. Pronounced gain around $\hbar\omega = 130$ meV sets in for current densities of several kA/cm². The height and width of the gain spectrum is in good agreement with the findings of [31].

² Terms of the form $z_{\mu\nu}\hat{O}_{\nu\mathbf{k},\mu'\mathbf{k}'}G_{\mu'\mu'}(\mathbf{k})\hat{O}_{\mu'\mathbf{k}',\mu\mathbf{k}}$ have been neglected for $\nu \neq \mu$ here. Their implication is not clear yet.

³ Note that J_0 also vanishes if the density matrix is diagonal in a basis of real states, which are not energy eigenstates. But then J_{scatt} no longer corresponds to the semiclassical result.

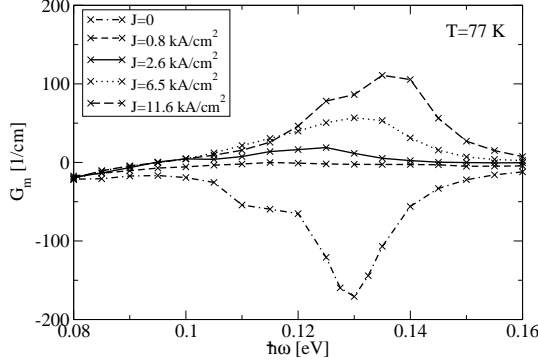


Fig. 4. Gain spectrum for the sample of [4] using $\gamma_{\text{imp}} = 0$. (From [29])

Within the semiclassical approximation the susceptibility is given by [32]

$$\Im\{\chi(\omega)\} = \sum_{\mu\nu\mathbf{k}} \frac{|\wp_{\mu\nu}|^2}{\epsilon_0 V} \frac{[f_\mu(\mathbf{k}) - f_\nu(\mathbf{k})](\Gamma_\nu + \Gamma_\mu)}{(E_\nu - E_\mu - \hbar\omega)^2 + (\Gamma_\nu + \Gamma_\mu)^2/4}, \quad (18)$$

where Γ_ν is the FWHM of $\Im\{G_{\nu\nu}^{\text{ret}}(\mathbf{k}, E)\}$ and $\wp_{\mu\nu} = ez_{\mu\nu}$ is the dipole matrix element. In [22] it was shown that this semiclassical approach gives reasonable results compared with the quantum model for the structure of [4].

In these approaches the influence of electron-electron interaction was totally neglected. Here we study the influence of many-particle corrections within the Hartree Fock approximation on the gain spectrum. The susceptibility is decomposed by

$$\chi(\omega) = 2(\text{for spin}) \sum_{\mu,\nu,\mathbf{k}} \wp_{\mu\nu} \chi_{\nu,\mu}(\mathbf{k}, \omega)$$

where the susceptibility functions $\chi_{\nu,\mu}(\mathbf{k}, \omega)$ between the eigenstates ν and μ are determined by the equation

$$\begin{aligned} \wp_{\nu\mu}(\mathbf{k}) (f_\nu(\mathbf{k}) - f_\mu(\mathbf{k})) = & \hbar(\omega - e_\nu(\mathbf{k}) + e_\mu(\mathbf{k}) + i(\Gamma_\mu + \Gamma_\nu)/2) \chi_{\nu\mu}(\mathbf{k}, \omega) \\ & + (f_\nu(\mathbf{k}) - f_\mu(\mathbf{k})) 2V \begin{pmatrix} \nu & \mu & \mu & \nu \\ & & 0 & \end{pmatrix} \sum_{\mathbf{k}'} \chi_{\nu\mu}(\mathbf{k}', \omega) \\ & - (f_\nu(\mathbf{k}) - f_\mu(\mathbf{k})) \sum_{\mathbf{k}'} \chi_{\nu\mu}(\mathbf{k}', t) V \begin{pmatrix} \nu & \nu & \mu & \mu \\ & \mathbf{k} - \mathbf{k}' & & \end{pmatrix}. \end{aligned} \quad (19)$$

Equation (19) reduces, in the equilibrium case, with only two isolated subbands of idealized quantum well subbands where phenomenological dephasing characterizes the broadening, to Eq. (5) of [33]. The bare Coulomb interaction and renormalized energies which appear above are given by

$$V \begin{pmatrix} \mu & \nu & \alpha & \beta \\ & \mathbf{k} - \mathbf{k}' & & \end{pmatrix} = \int dz dz' \phi_\mu^*(z) \phi_\nu(z) \frac{e^2 e^{-|\mathbf{k}-\mathbf{k}'||z-z'|}}{2\epsilon_r \epsilon_0 A |\mathbf{k} - \mathbf{k}'|} \phi_\alpha^*(z') \phi_\beta(z')$$

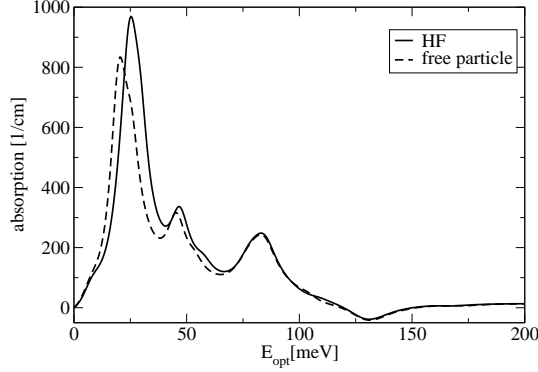


Fig. 5. Absorption spectrum for the sample from Fig. 2 with $N_d = 3.8 \times 10^{11}/\text{cm}^2$ at an operating field of $Fd = 0.2$ V. The dashed line gives the result from Eq. (18). The full line includes Coulomb corrections according to Eq. (19)

with the normalization area A and

$$\hbar e_\nu(\mathbf{k}) = E_\nu(\mathbf{k}) - \sum_{\mathbf{k}'} f_\nu(\mathbf{k}') V \left(\begin{smallmatrix} \nu & \nu & \nu & \nu \\ & \mathbf{k} - \mathbf{k}' \end{smallmatrix} \right) + \sum_{\mathbf{k}'} f_\nu(\mathbf{k}') V \left(\begin{smallmatrix} \nu & \mu & \mu & \nu \\ & \mathbf{k} - \mathbf{k}' \end{smallmatrix} \right).$$

The second term on the right-hand side of (19) gives rise to the depolarization shift [34,35], while the last term (exchange contribution) is analogous to the excitonic coupling term in interband transitions [36]. Figure 5 shows the absorption spectra. The inclusion of many-particle corrections yields a blue shift of about 5 meV for the low frequency absorption peak and a slight red shift for the gain peak around 130 meV.

6 Discussion

The impact of quantum effects on transport and gain in quantum cascade lasers have been examined. In the evaluation of the current two different terms, $J_0 \propto [\hat{H}_o, \hat{z}]$ and $J_{\text{scatt}} \propto [\hat{H}_{\text{scatt}}, \hat{z}]$ appear. In the semiclassical approximation, where the density matrix is assumed to be diagonal in the basis of energy eigenstates, J_{scatt} carries the entire current. Our quantum transport calculations show that J_{scatt} dominates the behavior for the prototype sample of [4], which has been frequently studied, thus justifying the semiclassical approaches in [19,20]. On the other hand the current J_0 , resulting from nondiagonal elements in the density matrix, shows strong contributions for the THz-laser of [9]. Nevertheless, it is not clear by now in how far the assumption of diagonal self-energies in the Wannier basis affects this behavior. Ongoing work is focused towards the inclusion of the full matrix structure in the self-energies.

The many particle effects are extremely dependent on the structure, since its design determines the actual electronic overlap and subband occupation. For the case considered here, the gain spectra are hardly modified by the electron-electron interactions within the Hartree-Fock approximations, while a significant depolarization shift occurs for the low frequency absorption.

Helpful discussions with M. Giehler, H.T. Grahn, A. Knorr, L. Schrottke, and M. Wörner as well as financial support by DFG within FOR394 is gratefully acknowledged.

Appendix

Similarly to [22] the scattering current (7) can be evaluated in the following way: We define the contour-ordered Green function (superscript c)

$$F_{\alpha\mathbf{k}}^c(\tau_1, \tau_2) = \sum_{\gamma\beta\mathbf{k}'} -i\hat{T}_c \{ \langle \hat{O}_{\alpha\mathbf{k},\beta\mathbf{k}'}(\tau_1) z_{\beta\gamma} \hat{a}_{\gamma\mathbf{k}'}(\tau_1) \hat{a}_{\alpha\mathbf{k}}^\dagger(\tau_2) \\ - z_{\alpha\beta} \hat{O}_{\beta\mathbf{k},\gamma\mathbf{k}'}(\tau_1) \hat{a}_{\gamma\mathbf{k}'}(\tau_1) \hat{a}_{\alpha\mathbf{k}}^\dagger(\tau_2) \rangle \}.$$

They are evaluated in the Dirac representation (with index D)

$$F_{\alpha\mathbf{k}}^c(\tau_1, \tau_2) = \sum_{\gamma\beta\mathbf{k}'} -i\hat{T}_c \left\langle e^{\int d\tau \frac{1}{i\hbar} \hat{H}_{\text{scatt}}(\tau)} \left\{ \hat{O}_{\alpha\mathbf{k},\beta\mathbf{k}'}^D(\tau_1) Z_{\beta\gamma} \hat{a}_{\gamma\mathbf{k}'}^D(\tau_1) \hat{a}_{\alpha\mathbf{k}}^{D\dagger}(\tau_2) \right. \right. \\ \left. \left. - Z_{\alpha\beta} \hat{O}_{\beta\mathbf{k},\gamma\mathbf{k}'}^D(\tau_1) \hat{a}_{\gamma\mathbf{k}'}^D(\tau_1) \hat{a}_{\alpha\mathbf{k}}^{D\dagger}(\tau_2) \right\} \right\rangle$$

The lowest order non-vanishing terms of the expansion gives

$$F_{\alpha\mathbf{k}}^c(\tau_1, \tau_2) \approx \sum_{\gamma\beta\mathbf{k}'} \frac{1}{\hbar} \sum_{\delta\epsilon} \int d\tau \\ \left\langle \hat{O}_{\alpha\mathbf{k},\beta\mathbf{k}'}(\tau_1) z_{\beta\gamma} G_{\gamma,\delta}^{c0}(\mathbf{k}'; \tau_1, \tau) \hat{O}_{\delta\mathbf{k}',\epsilon\mathbf{k}}(\tau) G_{\epsilon,\alpha}^{c0}(\mathbf{k}; \tau, \tau_2) \right. \\ \left. - z_{\alpha\beta} \hat{O}_{\beta\mathbf{k},\gamma\mathbf{k}'}(\tau_1) G_{\gamma,\delta}^{c0}(\mathbf{k}'; \tau_1, \tau) \hat{O}_{\delta\mathbf{k}',\epsilon\mathbf{k}}(\tau) G_{\epsilon,\alpha}^{c0}(\mathbf{k}; \tau, \tau_2) \right\rangle$$

with the bare Green functions $G_{\alpha,\gamma}^{c0}(\mathbf{k}; \tau_1, \tau) = -i\hat{T}_c \{ \langle \hat{a}_{\alpha\mathbf{k}}^D(\tau_1) \hat{a}_{\gamma\mathbf{k}}^{D\dagger}(\tau) \rangle \}$. In order to be consistent with the perturbation expansion in the Green functions, further terms are taken into account, which replace the bare Green functions by the full Green functions. Then we find

$$F_{\alpha\mathbf{k}}^c(\tau_1, \tau_2) \approx \frac{1}{\hbar} \sum_{\epsilon} \int d\tau \left[\Sigma_{\alpha\epsilon}^{cz}(\mathbf{k}; \tau_1, \tau) G_{\epsilon,\alpha}^c(\mathbf{k}; \tau, \tau_2) \right. \\ \left. - \sum_{\beta} z_{\alpha\beta} \Sigma_{\beta\epsilon}^c(\mathbf{k}; \tau_1, \tau) G_{\epsilon,\alpha}^c(\mathbf{k}; \tau, \tau_2) \right]$$

with

$$\Sigma_{\alpha\epsilon}^{cz}(\mathbf{k}; \tau_1, \tau) = \sum_{\gamma\beta\delta\mathbf{k}'} \langle \hat{O}_{\alpha\mathbf{k},\beta\mathbf{k}'}(\tau_1) z_{\beta\gamma} G_{\gamma,\delta}^c(\mathbf{k}'; \tau_1, \tau) \hat{O}_{\delta\mathbf{k}',\epsilon\mathbf{k}}(\tau) \rangle \quad (20)$$

where the averaging refers to the phonon bath for phonon scattering. Thus, in Born approximation the self energies Σ^z are given the the usual functionals for the self-energies $\Sigma(\mathbf{G})$ where the Green functions \mathbf{G} are replaced by

$\mathbf{Z} \cdot \mathbf{G}$ in matrix notation. Using Langreth rules and changing to the energy representation $F_{\alpha\mathbf{k}}^<(t, t)$ can be inserted in Eq. (7) yielding the final expression

$$\begin{aligned}
 J_{\text{scatt}} &= \frac{2e}{V\hbar} \sum_{\alpha\mathbf{k}} F_{\alpha\mathbf{k}}^<(t, t) \\
 &= \frac{2e}{V\hbar} \sum_{\alpha\mathbf{k}} \int \frac{dE}{2\pi} \left\{ \right. \\
 &\quad \sum_{\epsilon} \left[\Sigma_{\alpha\epsilon}^<(\mathbf{k}, E) G_{\epsilon, \alpha}^{\text{adv}}(\mathbf{k}, E) + \Sigma_{\alpha\epsilon}^{\text{ret}}(\mathbf{k}, E) G_{\epsilon, \alpha}^<(\mathbf{k}, E) \right] \\
 &\quad \left. - \sum_{\epsilon\beta} z_{\alpha\beta} \left[\Sigma_{\beta\epsilon}^<(\mathbf{k}, E) G_{\epsilon, \alpha}^{\text{adv}}(\mathbf{k}, E) + \Sigma_{\beta\epsilon}^{\text{ret}}(\mathbf{k}, E) G_{\epsilon, \alpha}^<(\mathbf{k}, E) \right] \right\}
 \end{aligned} \tag{21}$$

to evaluate J_{scatt} .

References

1. J. Faist, F. Capasso, D. L. Sivco, C. Sirtori, A. L. Hutchinson, and A. Y. Cho, *Science* **264**, 553 (1994).
2. M. Beck, D. Hofstetter, T. Aellen, J. Faist, U. Oesterle, M. Illegems, E. Gini, and H. Melchior, *Science* **295**, 301 (2002).
3. R. Köhler, A. Tredicucci, F. Beltram, H. E. Beere, E. H. Linfield, A. G. Davies, D. A. Ritchie, R. C. Iotti, and F. Rossi, *Nature* **417**, 156 (2002).
4. C. Sirtori, P. Kruck, S. Barbieri, P. Collot, J. Nagle, M. Beck, J. Faist, and U. Oesterle, *Appl. Phys. Lett.* **73**, 3486 (1998).
5. G. Scamarcio, F. Capasso, J. Faist, C. Sirtori, D. L. Sivco, A. L. Hutchinson, and A.-Y. Cho, *Appl. Phys. Lett.* **70**, 1796 (1997).
6. G. Strasser, S. Gianordoli, L. Hvozda, W. Schrenk, K. Unterrainer, and E. Gornik, *Appl. Phys. Lett.* **75**, 1345 (1999).
7. M. C. Wanke, F. Capasso, C. Gmachl, A. Tredicucci, D. L. Sivco, A. L. Hutchinson, S.-N. G. Chu, and A. Y. Cho, *Appl. Phys. Lett.* **78**, 3950 (2001).
8. N. Ulbrich, G. Scarpa, G. Böhm, G. Abstreiter, and M. Amann, *Appl. Phys. Lett.* **80**, 4312 (2002).
9. B. S. Williams, H. Callebaut, S. Kumar, Q. Hu, and J. L. Reno, *Appl. Phys. Lett.* **82**, 1015 (2003).
10. F. Capasso, J. Faist, and C. Sirtori, *J. Math. Phys.* **37**, 4775 (1996).
11. D. Paulavičius, V. Mitin, and M. A. Strosio, *J. Appl. Phys.* **84**, 3459 (1998).
12. S. Slivken, V. I. Litvinov, M. Razeghi, and J. R. Meyer, *J. Appl. Phys.* **85**, 665 (1999).
13. P. Hyldgaard and J. W. Wilkins, *Phys. Rev. B* **53**, 6889 (1996).
14. P. Harrison, *Appl. Phys. Lett.* **75**, 2800 (1999).
15. V. M. Apalkov and T. Chakraborty, *Appl. Phys. Lett.* **78**, 1973 (2001).
16. S. Tortora, F. Compagnone, A. Di Carlo, P. Lugli, M. T. Pellegrini, M. Troccoli, and G. Scamarcio, *Physica B* **272**, 219 (1999).
17. R. C. Iotti and F. Rossi, *Appl. Phys. Lett.* **76**, 2265 (2000).
18. R. C. Iotti and F. Rossi, *Appl. Phys. Lett.* **78**, 2902 (2001).
19. K. Donovan, P. Harrison, and R. W. Kelsall, *J. Appl. Phys.* **89**, 3084 (2001).

20. R. C. Iotti and F. Rossi, Phys. Rev. Lett. **87**, 146603 (2001).
21. A. Wacker, in *Advances in Solid State Physics*, edited by B. Kramer (Springer, Berlin, 2001), p. 199.
22. S.-C. Lee and A. Wacker, Phys. Rev. B **66**, 245314 (2002).
23. T. Kuhn, in *Theory of Transport Properties of Semiconductor Nanostructures*, edited by E. Schöll (Chapman and Hall, London, 1998).
24. L. P. Kadanoff and G. Baym, *Quantum Statistical Mechanics* (Benjamin, New York, 1962).
25. L. V. Keldysh, Sov. Phys. JETP **20**, 1018 (1965), [Zh. Eksp. Theor. Fiz. **47**, 1515 (1964)].
26. H. Haug and A.-P. Jauho, *Quantum Kinetics in Transport and Optics of Semiconductors* (Springer, Berlin, 1996).
27. A. Wacker, Phys. Rep. **357**, 1 (2002).
28. M. Giehler, R. Hey, H. Kostial, S. Cronenberg, T. Ohtsuka, L. Schrottke, and H. T. Grahn, Appl. Phys. Lett. **82**, 671 (2003).
29. A. Wacker, Phys. Rev. B **66**, 085326 (2002).
30. J. D. Jackson, *Classical Electrodynamics*, 3 ed. (John Wiley & Sons, New York, 1998).
31. F. Eickemeyer, R. A. Kaindl, M. Woerner, T. Elsaesser, S. Barbieri, P. Kruck, C. Sirtori, and J. Nagle, Appl. Phys. Lett. **76**, 3254 (2000).
32. H. Haug and S. W. Koch, *Quantum Theory of the Optical and Electronic Properties of Semiconductors*, 2 ed. (World Scientific, Singapore, 1993).
33. S. L. Chuang, M. S. C. Luo, S. Schmitt-Rink, and A. Pinczuk, Phys. Rev. B **46**, 1897 (1992).
34. T. Ando, A. B. Fowler, and F. Stern, Rev. Mod. Phys. **54**, 437 (1982).
35. M. Helm, in *Intersubband Transitions in Quantum Wells: Physics and Device Applications*, edited by E. R. Weber and R. K. Willardson (Academic Press, 1999), Vol. 62, p. 1.
36. M. F. Pereira, Jr., R. Binder, and S. W. Koch, Appl. Phys. Lett. **64**, 279 (1994).